Atom Indonesia

Journal homepage: http://aij.batan.go.id

Elemental Mapping for Characterizing of Thorium and Rare Earth Elements (REE) Bearing Minerals Using μXRF

I. G. Sukadana[1,2*], I. W. Warmada[1], F. Pratiwi[2], A. Harijoko[1], T. B. Adimedha[2], A. W. Yogatama[3]

[1]*Department of Geological Engineering, Faculty of Engineering, Universitas Gadjah Mada, Yogyakarta 55281, Indonesia*
[2]*Research Center for Nuclear Minerals Technology, National Research and Innovation Agency (BRIN), Jl. Lebak Bulus Raya No. 9, Pasar Jumat, Jakarta Selatan 12440, Indonesia*
[3]*PT. Timah, Tbk., Pangkal Pinang, Bangka Belitung Archipelago 33121, Indonesia*

ARTICLE INFO

Article history:
Received 17 January 2022
Received in revised form 24 March 2022
Accepted 19 April 2022

Keywords:
Thorium
REE
Micro XRF
AMICS
Mamuju

ABSTRACT

Thorium (Th) anomaly was found in Adang Volcanic Complexes, Mamuju Area, West Sulawesi. This element is associated with high-value elements, the rare earth elements (REE). The minerals containing Th and REE were found in veins mineralization with various types of minerals which are very difficult to identify by conventional method. This research aims to understand the distribution and characterization of Th and REE in individual minerals, using Micro X-Ray Fluorescence (μXRF) analysis and completed by Advanced Minerals Identification and Characterization System (AMICS) software. The samples were collected from vein mineralization in Hulu Mamuju Sector. The contents of Th and REE that were analyzed using X-Ray Fluorescence (XRF) completed by Inductively Coupled Plasma Mass Spectrometry (ICP-MS) are 11,550-74,480 ppm and 6,244.15-48,036.87 ppm, respectively. The minerals that contain Th and REE are britholite ($(Ce,Ca)_5(SiO_4)_3OH$), aeschynite $(Ce,Ca,Fe,Th)(Ti,Nb)_2$ $(O,OH)_6$, cerite $(Ce,Ca)_9(Mg,Fe)(SiO_4)_3(HSiO_4)_4(OH)_3$, monazite $(REE,Th(PO_4))$, thorite $(Th(SiO_4))$, and thorutite $(Th,U,Ca)Ti_2(O,OH)_6$ associated with other minerals such as pyrite, actinolite, apatite, ilmenite, hematite, zircon and ankerite. Some minerals are uncommon minerals and are only characterized by detailed elemental mapping. The variety of minerals shows the condition of mineralization influenced by carbonatite magma and the hydrothermal process of mineralization.

INTRODUCTION

Thorium (Th) can be a part of energy future as it can be transmuted into fissile U-233, although it is still on progress to replace the primary nuclear energy source, that is U-235 [1]. The occurrences of thorium found in the Mamuju Area are associated with other valuable elements, such as Rare Earth Elements (REE) [2]. The high content of Th and REE distribution in this area is reflected by a high anomaly of radiation dose rate and thorium anomaly (more than 700 nSv/h, refer to annual dose rate 5 mSv/y) [3].

Based on radiometric and regional geochemical data, the most intriguing area with the highest content of thorium radionuclide (eTh) is found in Hulu Mamuju Sector [3,4]. The identification of specific minerals containing radioactive minerals in this area, uranium (U) and Th, was conducted by point analysis using SEM-EDS and resulted in thorianite (ThO_2) [5]. This mineral is considerably difficult to identify and characterize with microscopic and conventional equipment. The process of ore processing requires information regarding the distribution of elements in minerals, the process of mineralization and alteration, the elements distribution, and type of ore minerals [6]. Understanding mineral distributions in rocks also has a particular value to the mineral processing industry, where ascertaining the distribution of minerals in an economic deposit could be beneficial to defining and estimating the mineral resources, or more efficient for ore processing [7].

*Corresponding author.
E-mail address: sukadana@batan.go.id
DOI: https://doi.org/10.17146/aij.2022.1215

This study aims to evaluate the high content of Th and REE in vein ore and characterize the both the element and mineral distribution. Elemental mapping was conducted by micro-XRF M4 Tornado plus with a 20 µm collimator using an area mapping system to determine the distribution of elements and elements combination. This data was completed by advanced minerals identification and characterization system (AMICS) software to identify and characterize the specific mineral containing Th and REE and the distribution of minerals in the ore. This method has been successfully applied in the characterization of Cu distribution in soil [8], characterizing the carlin gold deposits type with precise determination of mineralogy, element distribution and mineralogy texture which undefined with naked eyes [7], uranium, thorium identification [9], and other geological material due to the qualitative and quantitative advantages it possesses [10].

This study will become the reference to the processing and beneficiation of Th and REE from the ore. This study is focused on the mineralization area in the Hulu Mamuju sector as an exploration prospect of Th and REE as structure-bound volcanic-related types.

Regional geology

Tectonic setting and magmatism in West Sulawesi have correlated with the post-collision in the east of Sulawesi and development of Makassar Strait in the west part of Sulawesi [11]. The volcanic rocks in the west part of Sulawesi are composed of alkaline volcanic rocks as the product of post-collision and also have the signature of subduction product caused by the oceanic crust lies beneath the micro continental crust [11-17].

Furthermore, the geochemical signature of the volcanic rocks indicates the silicate melting caused by the strong enrichment in Na, K, Zr, and REEs [16,18,19]. Advanced magma mixing such as crystal fractionation including, the fractionation of leucite and alkali feldspar, continent crust assimilation, give significant contributions to the Adang Volcanic Complexes (AVC) geochemical signature [20,21]. Metasomatic process and continental crust contamination can be observed from elevated concentrations of trace elements such as Mg, Ni, and Cr linear with the elevated of K, LREE, and LILE [22]

The Th and REE exploration target are grouped in the Miocene Adang Volcanic Complexes (AVC) Fig. 1 [2,23,24]. The complex is located in the Mamuju Region, West Sulawesi, Indonesia. The AVC is divided into various rock units with some volcanic eruption centers and is underlay by young sedimentary units [24]. The primary target is the distribution of volcanic rocks, especially ultra-potassic rocks, namely the Hulu Mamuju Sector [25,26].

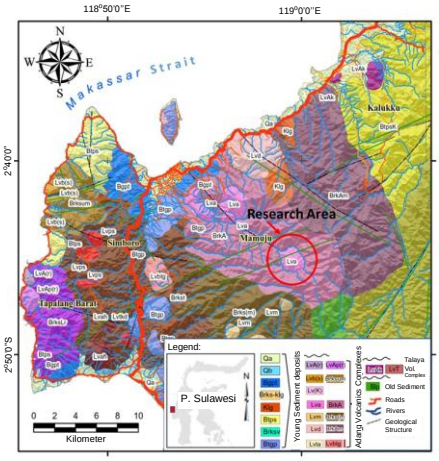

Fig. 1. Research location combined with detailed geological Map of Mamuju Area, (base map sources: https://tanahair.indonesia.go.id/demnas/#/demnas) [24].

The aforementioned sector is composed of trachyte, phonolite, and syenite rocks. The mineralization is found in contact with syenite and phonolite lava. The mineralization is usually found in structures that correlated with the contact (Fig. 2). The structure is dominantly normal fault with the various pattern and dimensions. The mineralization was found as a fracture filling vein with high radiometric value. The detailed description of every single vein including the position, host rock/lithology, radiometric dose rate value, and the dimension of mineralization vein is explained in Table 1.

Table 1. The characteristic of the vein with radiometric anomaly.

Code	Morphology/Structure	Lithology	Radiometry Dose rate	Vein Dimension
MV 0	Cliff with vein pattern N135◦E	Phonolite lava	145 µSvh^{-1}	2 m × 15 m
MV1	The small hills with vein trend N240◦E	Phonolite lava, direct contact with syenites	177.3 µSvh^{-1}	4 m × 150 m
MV2	The vein found upper the small river	Phonolite lava	46.4 µSvh^{-1}	2 m × 8 m
MV3	Mineralization found on the cliff of the river found in weathered rocks with un-oriented vein	Alteration of phonolite lava	149.8 µSvh^{-1}	2.5 m × 8 m
MV4	The ridge of the hill and intensive fracture with vein pattern N245◦E	Very intensive alteration of phonolite lava	>1.1 mSvh^{-1}	2 m × 12 m
MV5	The ridge of the hill and intensive fracture with vein pattern N250◦E	Very intensive alteration of phonolite lava	416 µSv^{-1}	2.5 m × 8 m
MV6	Cliff in the western part of the hill with vein pattern N305◦E	Phonolite lava	176.9 µSv^{-1}	1.5 m × 12 m
MV7	The cliff in the western hillside of the dome with vein N295◦E	Phonolite lava	147.3 µSvh^{-1}	2 m × 15 m

METHODOLOGY

The Th and REE mineralization with vein system was found in Hulu Mamuju Sector, Mamunyu village, with a high radiometric dose rate. Therefore, the research area was focused in this sector with detailed fieldwork and sampling to identify Th and REE-bearing minerals. Every location of the mineralization outcrop has been trenched and characterized by the in-situ description method. Every trenched location was conditioned by pilling the overburden soil until the mineralization can be characterized, either vein or ore mineralization, and the pattern of geological structure as the initial fracture can be identified. Identification was completed by detailed radiometric measurement using RS 125 with static measurement for about 60 seconds and grinding measurement for about 1 m. After figuring out the zone of mineralization and characterization of hand specimens of ore, the fieldwork continued by chip sampling and location notification. The figure out of mineralization trenching is shown in Fig. 2**.**

(a) (b)

Fig. 2. The figure out of mineralization. a). Trenching of MV4 showing anomaly with radiometric dose rate 1,1 mSv/h and the radio-element content higher than the detection limit (>1 % of eU and eTh), and b). MV1 trenching with 2,5 m wide and >50 m long and the radioelements content are 1364 ppm eU and >1 % eTh.

The ore sample came from the vein with high radioactivity exposure, and the outcrop was trenched and identified using gamma-ray detector RS 125 and SPP2NF scintillometer. The identification of samples was carried out in the location by sketch, accompanied by recording the coordinate location, radiometric value, and sample description. Detailed sampling was conducted to get the representative sample, and eight selected samples were taken from different veins. The purpose of the selected sample is to get the representative and perfect kind of minerals to identify the distribution of elements and characteristics of the ore. Based on the radiometric anomaly value, there are eight representative samples. The samples are representations of different ore veins, with samples code are MV0, MV1, MV2, MV3, MV4, MV5, MV6, MV7 with the description of mineralization zone shown in Table 1. The sample location and detailed geological map are shown in Fig. 3.

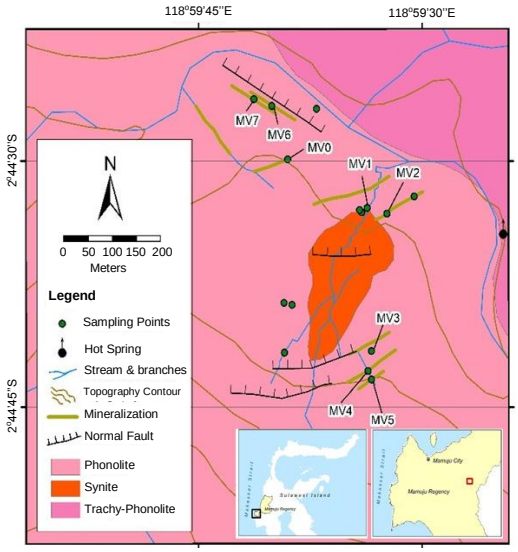

Fig. 3. Detailed geological map and sampling location in Hulu Mamuju Sector, West Sulawesi (Base map sources: https://tanahair.indonesia.go.id/demnas/#/demnas).

For the eight selected samples, several combined analyses were carried out to characterize the ore containing significant Th and REE. Eight samples with a relatively high value of radioactivity dose rate were analyzed using petrography and XRF spectrometry in the National Nuclear Minerals Laboratory, National Nuclear Energy Agency of Indonesia (BATAN), and ICP-MS in Intertek Utama Services laboratory.

Geochemistry analysis using XRF analysis was measured by Desktop XRF (Xepos, Ametek, Berwyn, PA, USA) to determine major oxide, traces, and some REEs in the samples. The samples were air-dried at 25-35 °C for three days and then oven-dried at 105 °C for around 24 hours to remove the moisture content until a constant weight was reached. The samples were crushed and mashed to a size of 200 mesh and heated at 105 °C for 2 hours to remove organic compounds. A total of 5 g of each sample was weighed, and 1 g of lithium tetraborate ($Li_2B_4O_7$; Merck, Darmstadt, Germany) was added as a binding agent. The mixture was stirred and compressed into a pellet, then analyzed using XRF. Before testing the samples, XRF calibration was performed using some calibration samples, such as a blank, OREAS-124 (Mantra Resources Nyota Prospect, Lindi, Tanzania), OREAS-465 (Tanzania-Mantra Resources Nyota Prospect), and GSR-5 (China).

ICP-MS analysis was conducted in Intertek Utama Services laboratory that has Quality Assurance expertise in elemental trace and ultra-trace analysis. The mineralogy analysis was conducted by petrographic analysis combined with elemental mapping and AMICS (Advanced Minerals Identification and Characterization

System). The analysis of petrographic thin section was done using an optical, polarization microscope to identify the characterization of mineralogy and rock texture [27,28]. The method shows the mineral's descriptions of the shape, size, intergrowth between minerals, and the presence of inclusions and also the relationships between minerals.

Elemental mapping was analyzed using the μ-XRF instrument in BATAN (M4 Tornado Plus, produced by Bruker Nano). This equipment system has a double microprobe with an Rh X-ray tube. Poly-capillary optics provide an X-ray beam with a diameter of 20 μm on the sample. The energy of the X-ray tube can operate up to 50 kV and 600 μA, although the transmission function of the poly-capillary optics is low for higher energies, limiting the range of high-energy lines that can be excited, e.g., Ba K-lines at ~32-36 keV are not excited to a detectable level. The sample chamber (300 mm × 120 mm × 260 mm), can be used for analysis of the large samples, and it can be conducted at atmospheric pressure or under an oil-free and controlled vacuum by the use of a pressure-controlled diaphragm pump. All the analyses in this study were carried out at a 20 mbar vacuum. The sample width was 2 × 2 cm (by 20 pixels) [29-31].

The AMICS software can identify mineral groups (mixtures) and a single mineral in each sample. The method has multiple mineral labels and abundances for each pixel and provides a single label per pixel. AMICS software give results for mineral identification with the characterization of elements set spectrum in every single pixel. In the case of multiple minerals in one pixel, the software will label the pixel by the single dominant mineral (representing one or more combined minerals). However, even those mineral classes that were identified as a single mineral (i.e., leucite) have photon energy peaks from additional elements (e.g., K and Al). As there is no way to classify the fast number of possible mixture variations when three or four minerals may be mixed, mineral mixtures for fine-grained (less than 20 microns) samples cannot be accurately quantified using the AMICS method. The list of samples and the types of analysis are shown in Table 2.

Table 2. The list of samples and laboratory methods.

Sample	XRF	ICP-MS	Petro graphic	Micro-XRF Mapping	AMICS
MV0	√	√	√	√	√
MV1	√	√	√	-	-
MV2	√	√	√	√	√
MV3	√	√	√	√	√
MV4	√	√	√	√	√
MV5	√	√	√	-	-
MV6	√	√	√	√	√
MV7	√	√	√	√	√

The minerals containing REE and/or Th are usually found in some minerals (Table 3) with different grades and formulas, mainly oxides, silicates, phosphates, and fluoro-carbonates depending on the type of the host rock [32].

Table 3. List of minerals containing REE [32].

Mineral	Formula	Approx. TREO (wt.%)
Allanite	$(Y,Ln,Ca)_2(Al,Fe^{3+})_3(SiO_4)_3(OH)$	39
Apatite	$(Ca,Ln)_5(PO_4)_3(F,Cl,OH)$	19
Bastnäsite	$(Ln, Y)(CO_3)F$	75
Eudialyte	$Na_4(Ca,Ln)_2(Fe^{2+},Mn^{2+},Y)$ $ZrSi_8O_{22}(OH,Cl)_2$	9
Fergusonite	$(Ln, Y)NbO_4$	53
Gittinsite	$CaZrSi_2O_7$	
Iimoriite	$Y_2(SiO_4)(CO_3)$	68
Kainosite	$Ca_2(Y,Ln)_2Si_4O_{12}(CO_3)\cdot H_2O$	38
Loparite	$(Ln,Na,Ca)(Ti,Nb)O_3$	30
Monazite	$(Ln, Th)PO_4$	65
Mosandrite	$(Na,Ca)_3Ca_3Ln$ $(Ti,Nb,Zr)(Si_2O_7)_2(O,OH,F)_4$	33
Parisite	$Ca(Ln)_2(CO_3)_3F_2$	61
Pyrochlore	$(Ca,Na,Ln)_2Nb_2O_6(OH,F)$	
Rinkite (rinkolite)	$(Ca,Ln)_4Na(Na,Ca)\ 2Ti(Si_2O_7)_2(O,F)_2$	20
Steenstrupine	$Na_{14}Ln_6Mn_2Fe_2(Zr,Th)(Si_6O_{18})2(PO_4)_7\cdot 3H_2O$	31
Synchysite	$Ca(Ln)(CO_3)_2F$	51
Xenotime	YPO_4	61
Zircon	$(Zr, Ln)SiO_4$	4

RESULTS

A series of analysis were carried out on 8 (eight) vein samples with high radioactivity. Initial analysis was carried out with a geochemical analysis of rocks using XRF and ICP-MS. The analysis was continued with mineralogy analysis using petrographic and detailed analysis by elemental mapping using μXRF. The final analysis performed is mineral analysis with AMICS.

Geochemistry

XRF and ICP-MS analysis

The eight samples were analyzed for the major, trace, and rare earth elements. The trace elements contents are elevated significantly until a thousand times, especially Zr, Ba, Th, and U, with the highest value of 8,305 ppm, 3,398 ppm, 74,480 ppm, and 5,769 ppm, respectively. The high content value of the trace element is followed by REE levels. The value of yttrium and light REE elevated thousands of times and for heavy REE elevated hundreds of times. The complete analysis result is shown in Table 4.

Table 4. Trace and Rare Earth elements from XRF and ICP-MS Analysis.

Samples	MV0	MV1	MV2	MV3	MV4	MV5	MV6	MV7
SiO_2 (%)	49.19	53.83	14.74	53.88	50.27	43.07	36.58	34.35
TiO_2 (%)	0.24	0.63	3.51	0.30	1.12	2.05	1.10	2.52
Al_2O_3 (%)	18.94	20.35	2.51	20.00	17.26	16.95	11.63	12.52
Fe_2O_3 (%)	6.20	4.37	14.57	5.02	9.04	17.46	7.01	27.46
MnO (%)	0.04	0.03	0.15	0.05	0.01	0.70	0.13	0.29
MgO (%)	0.87	1.68	1.71	0.69	0.57	4.63	1.72	1.46
CaO (%)	0.86	1.64	25.28	0.72	0.23	0.48	2.04	2.95
Na_2O (%)	0.94	2.45	2.19	0.75	0.66	0.75	1.85	1.64
K_2O (%)	8.94	8.36	1.58	10.38	11.20	7.91	6.82	6.62
P_2O_5 (%)	1.92	1.89	17.99	1.36	0.74	1.88	2.54	1.58
V (ppm)	893	621	878	706	318	863	1603	1,728
Co (ppm)	195	131	139	142	11	180	184	172
Zn (ppm)	213.2	93.5	97.4	177.1	23.9	355.4	87.2	275.3
Rb (ppm)	499.8	506	122.2	573.9	363.2	597.2	370.8	504.6
Sr (ppm)	915.5	1,210	12,110	657	55.6	424.2	1,108	2,058
Zr (ppm)	2,221	8,305	1,887	1,837	2,473	1,730	4,576	2,211
Nb (ppm)	252.9	521.5	2168	183.8	135.8	909.4	500.8	288.8
Ba (ppm)	1051	1229	1963	1372	1716	3398	1006	1466
Pb (ppm)	261.5	146.0	530.1	218.6	397.6	1.190.0	244.6	333.7
Th (ppm)	74,480.0	24,550.0	11,550.0	55,400.0	73,950.0	14,450.0	34,190.0	38,240.0
U (ppm)	2,102.0	1,326.0	5,769.0	1,714.0	7,035.0	1,222.0	1,838.0	1,566.0
Sc (ppm)	281.3	132.6	52.0	200.3	196.7	79.50	143.0	155.0
Y (ppm)	2,351.0*	2,101.0	1,057.0	1,433.0	581.9	1,007.0	2,427.0	1,728.0
La (ppm)	9,122.0*	1,500.0*	2,330.0*	7,095.0	1,058.0*	1,940.0*	10,380.0	7,110.0
Ce (ppm)	24,120.0*	3,100.0*	5,260.0*	18,170.0	3,379.0*	8,120.0	24,140.0	17,250.0
Pr (ppm)	1,250.0*	311.0*	609.0*	1,680.0*	189.0*	483.0*	1,277.0*	2,460.0*
Nd (ppm)	4,250.0*	983.0*	2,220.0*	5,727.0	633.0*	1,720.0*	5,817.0	4,205.0*
Sm (ppm)	727.0*	689.0*	302.0*	534.0 *	97.4*	289.0*	1,540.0*	1,430.0*
Eu (ppm)	127.0*	20.9*	65*	156*	15.9*	49.0*	259.0*	243.0*
Gd (ppm)	521.0*	70*	263*	580*	46.5*	199.0*	1.030.0*	944.0*
Tb (ppm)	58.4*	8.17*	28.4*	61.1*	5.6*	21.4*	113.0*	108.0*
Dy (ppm)	268.0*	38.1*	135*	268*	25.1*	101.0*	518.0*	522.0*
Ho (ppm)	39.7*	5.5*	19.8*	36.8*	3.3*	14.9*	76.5*	78.0*
Er (ppm)	100.0*	15.2*	51.3*	94.3*	7.9*	39.7*	198.0*	204.0*
Tm (ppm)	10.1*	1.9*	5.6*	10.4*	0.8*	4.6*	21.4*	22.0*
Yb (ppm)	39.6*	10.8*	23.0*	44.9*	3.7*	20.8*	89.0*	92.5*
Lu (ppm)	3.3*	1.45*	2.75*	4.02*	0.3*	2.1 *	8.0 *	8.3*
REE+Sc+Y (ppm)	**43,268.38**	**8,988.62**	**12,423.85**	**36,094.82**	**6,244.15**	**14,091.03**	**48,036.87**	**36,559.76**

Note: *) Analyzed by ICP-MS

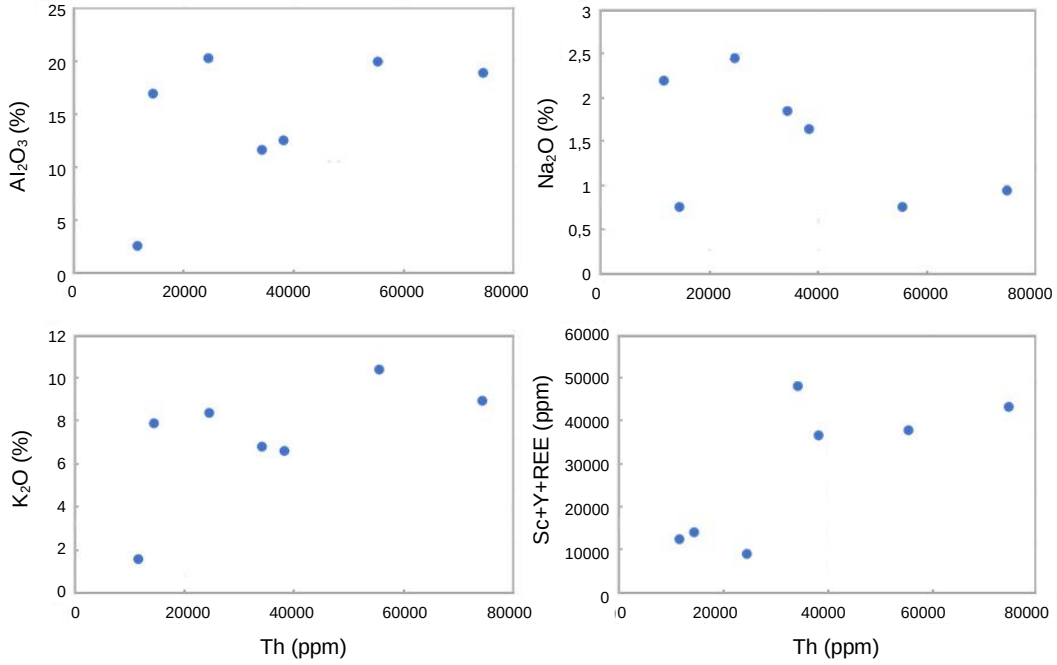

Fig. 4. The correlation between Th and other oxide and elements.

The geochemical analysis result also showed the value of Th content elevated significantly in the veins in the range from 1.1-7.4 % compared to the continental crust, with an average of Th content is 11 ppm [33]. The highest content is found in sample MV0. Th content has a positive correlation with other elements, such as major elements (K and Al) and trace elements (Sr, Rb, Zr) and TREY (REE+Y). However, there are also some negative correlations between Th with Na and Si (Fig. 4). The content of TREY is also elevated hundreds of time from chondrites rock [34]. The content of TREY is extremely high in all samples. Spider diagram in Fig. 5 shows the patterns of REE and Y content normalized by chondrites. It was figured out the occurrences of LREE on apatite group, light REE is extremely higher than heavy REE, with very strong variable La/Yb (75-280) and La/Tb (65-188). The patterns are indicated the intensive fractionation of LREE and HREE [35].

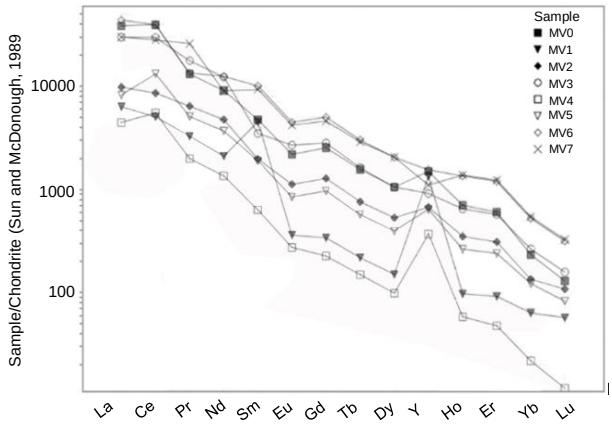

Fig. 5. Spider diagram of REE+Y+Sc content in every sample normalize by chondrites [34].

The result of the negative Eu anomaly is comparable with britholite mineral occurrences [36]. This indication will be guided to the next step of the analysis to concern the minerals that contain the light REE. The most significant positive anomaly of Y in samples MV1 and MV4 are indicated as the special mineral occurrences.

Mineralogy

Thin section analysis

Thin section analysis was conducted for some samples with high Th and REE content. The sample is generally altered and dominantly composed of clay minerals. The ore samples were altered with the dominance of chlorite and hematite minerals which gave the impression of a greenish-yellow color and red spots on the rock samples, the size of the minerals making up the rock are ranging from <0.1-0.5 mm. Greenish-yellow rock. The special texture of the rock is not observed, the texture of alteration minerals, inequigranular grain, with a short prismatic shape on the base mass and some parts in the form of equant crystals with a lezonge/diamond shape, panidiomorphic granular. The secondary minerals formed in sample BM 1 are chlorite, hematite, rutile, titanite, and altered calcite. In BM 2 sample consists of the secondary minerals namely actinolite, plagioclase, biotite, opaque minerals, and britholite. Sample ore BM 4 is an inequigranular grain, with a short prismatic shape on the base mass and some parts in the form of equant crystals with a lezonge/diamond shape, panidiomorphic granular. The secondary minerals formed are chlorite, hematite, rutile, titanite, and altered calcite.

The other sample is from the MV06 vein; the vein is dominated by opaque mineral (hematite) at the edge, and mineral aggregate of apatite group (britholite), zeolite, sericite, and opaque mineral on the inner side of the vein Fig. 6. Sample MV07 has been intensely altered, with pervasive alteration on both phenocrysts and groundmass, and has been cut by a vein. Phenocryst consists of biotite, pyroxene, aegirine, and green hornblende. Most of the phenocryst has been altered to secondary amphibole (tremolite-actinolite), with minor secondary biotite, calcite, apatite, cancrinite, and opaque mineral. The groundmass has been replaced by fibrous minerals (zeolite). The vein consists of opaque mineral (hematite) on the outer side, and mineral aggregate of apatite, zeolite, sericite, and opaque mineral (hematite) on the inner side of the vein.

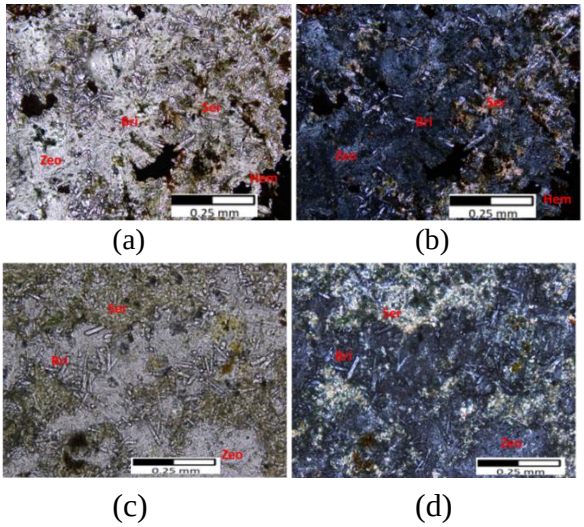

Fig. 6. The thin section image. a,b). parallel and crossed polarization of MV06 shown the alteration and distribution of britholite (Bri), zeolite (Zeo), and sericite (Ser), c,d). The parallel and crossed polarization of the MV07 thin section showed britholite (Bri), hematite (Hem), zeolite (Zeo), and sericite (Ser) with abbreviation according to IMA-CNMNC [37].

Micro x-ray fluorescence analysis (μ-XRF)

Some selected samples analyzed using XRF and ICP-MS were scanned using micro XRF. Micro XRF measurement of the ore sample begins with scanning the sample in the form of a polished section with a size of 20 × 20 mm and a pixel size of 20 microns. The scan results show the distribution of the element content in each pixel. Every sample has a unique characteristic of elements distribution and combination of the multi-element in every pixel.

From the result of micro-XRF scanning at the edge of the vein sample MV 7, high content of Fe and Ti are detected; based on the petrography this area is described as an opaque mineral (hematite). The area with high content of Th, P, Ca, and light REE, which predominantly Ce, Nd, and Y, is shown in Fig. 7. Besides the distribution of the single elements, the data can be overlay customized for multi-element distribution. This method can figure out the combination of elements in every pixel and the association and minerals constituent elements (Fig. 8). Based on the result, high content of P, Ca, and REE (Ce, Nd, Y) were found in form of lineaments pattern and spreading in the vein bodies. The high content of Fe, U, and Ti are concentrated at the edge of the vein, and the rest of the area contains high content of Si, Al, Ca, and K. In the MV 6 sample which was dominated by REE, the REE content was quite significant, including Ce (5.97 %), La (2.04 %), Nd (1.90 %) and Y (0.57 %), including Th (6.71 %) and U (0.36 %). The distribution of light REEY and Th has been separated from the distribution of Mg, Ti, and Si.

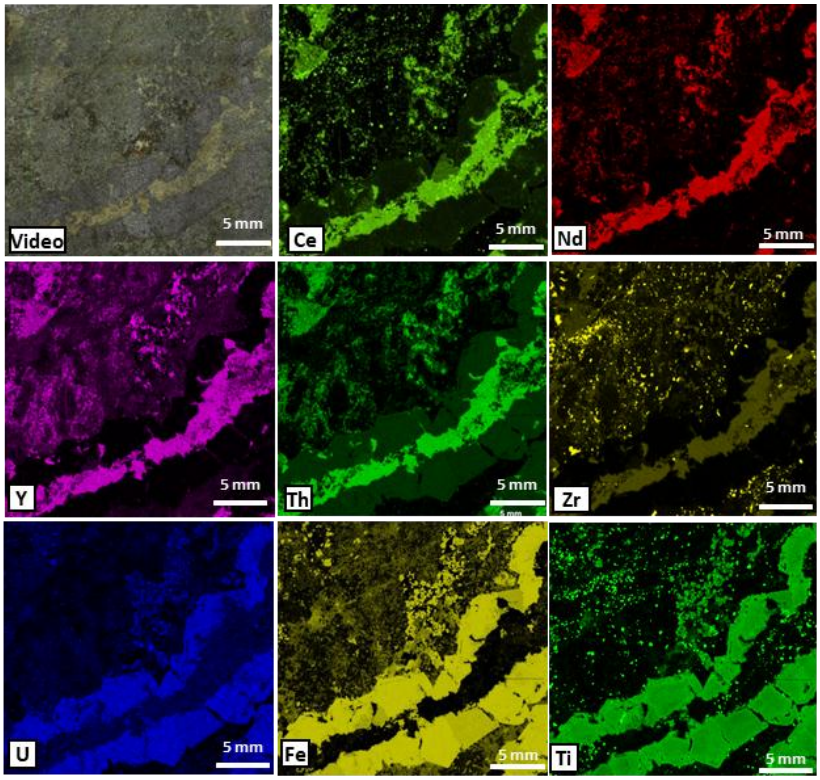

Fig. 7. Elemental mapping results show, the accumulation of radioactive elements (Th and U) and REE (Ce, Nd, and Y) in one mineral as phosphate form of minerals, but the association of Fe and Ti are accumulated in other minerals.

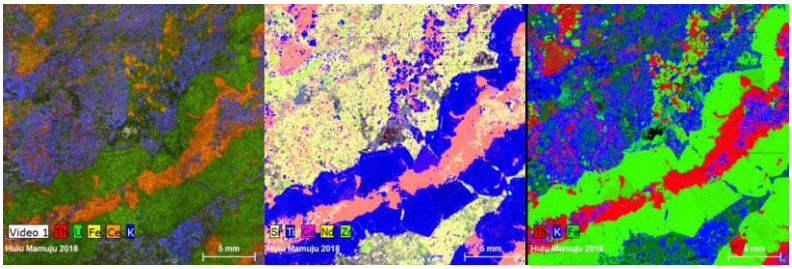

Fig. 8. The combination of MV7 elemental mapping results. The selected elements are, Th: Thorium; La: Lanthanum; Ce: Cerium; Ca: Calcium; P: Phosphate; Al: Alumina; Si: Silica; K: Potassium; Ti: Titanium; Fe: Iron; Nb: Niobium.

The distribution of Th also has different elements composition in MV 3 sample. Th content has the same distribution as P, Ce, Nd, La, and Si. The spectrum and composition of the pixel containing Th and associated elements are shown in Fig. 9. Every pixel has a specific spectrum and will be compared with the spectrum of the mineral standard database. All samples have been mapped and obtained elements composition for mineral analysis in every pixel.

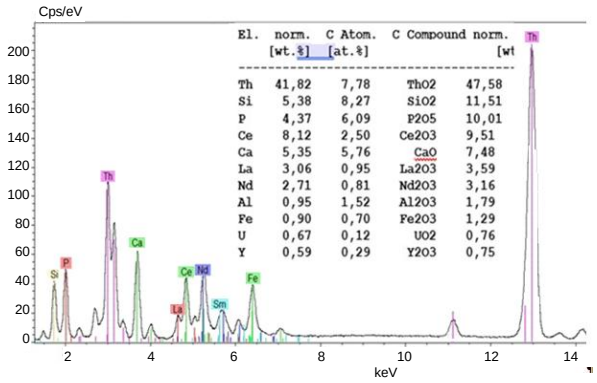

Fig. 9. The spectrum of the pixel containing Th, P, Si, Ce, La, and Nd.

Advanced minerals identification and characterization system (AMICS)

The results of the elemental mapping analysis were used for mineralogy identification using the AMICS software. This software uses a dataset from the measurement results of the M4 Tornado. The scanning results have obtained the composition spectrum of the elements combination in each pixel that shows the characteristics of the composition of a mineral. These spectra were compared with the standard spectra of minerals in the AMICS database [7,38,39]. From several samples that have been scanned using a micro XRF M4 Tornado plus tool and analyzed using AMICS, a list of minerals is obtained such as shown in Table 1.

Each mineral has a specific mineral composition characteristic. Several minerals containing REEY and Th obtained from scanning using M4 Tornado show the composition, distribution, and association of minerals. The mineral characteristics of each sample indicate that mineralization is formed in different phases and processes, so that the Th, Y, and REE-bearing minerals have different shapes, sizes, and associations.

In the MV7 sample there are minerals containing Th associated with Ca, Ce, Nd, and Y. These minerals have the same spectrum as the standard mineral in the database, namely britholite $(Ce,Ca,X)_5(SiO_4)_3(OH)$ [40]. Th and Y elements are substitute elements in this mineral, so their content can vary. This mineral forms inside the veins and is associated with other minerals such as titanite ($CaTi(SiO_4)O$), zircon ($Zr(SiO_4)$), and zeolite ($(K,Na)_5(Si_{31}Al_5)O_{72}\cdot 18H_2O$). The other dominant mineral distribution is hematite (Fe_2O_3) covering the oriented Th and REEY-bearing minerals. The distribution of hematite also spreads in the vein bodies associated with hedenbergite, wadeite, apatite, and ilmenite (Fig. 10).

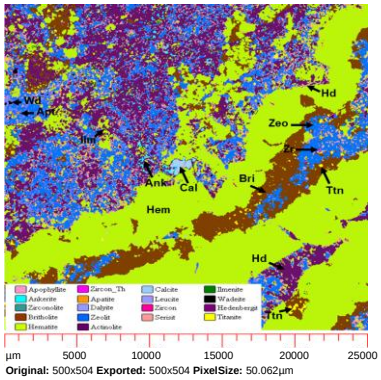

Fig. 10. The result of AMICS analysis for MV 7, there Britholite (Bri), Hematite (Hem), Actinolite (Act), Titanite (Ttn), Zeolite (Zeo), Calcite (Cal), Hedenbergite (Hd), Ankerite (Ank), and other minerals, with abbreviation according to IMA-CNMNC [37].

The combination of elemental distribution in the MV3 sample shows different REE and Th-bearing minerals. In this sample, Th is associated with light REE (La, Ce, Nd), Si, and P. The mineral composition is like the spectrum of monazite ($REE(PO_4)$) with a high Th content. The distribution of these minerals is associated with britholite and aeschynite ($(Ce,Ca,Fe,Th)(Ti,Nb)_2(O,OH)_6$). The MV3 ore body is dominated by the clay mineral, illite ($K_{0.65}Al_2.0[A_{l0.65}Si_{3.35}O_{10}](OH)_2$) as a product of mica alteration. This monazite distribution was cut by the hematite mineral that filled the new orientation of fracture. The other part of ore bodies is filled with orthoclase minerals associated with phlogopite, biotite, and ilmenite (Fig. 11).

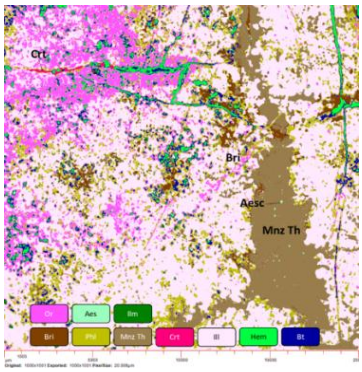

Fig. 11. The result of AMICS analysis for MV 3, there are: Orthoclase (Or), Aeschynite (Aes), Ilmenite (Ilm), Britholite (Bri), Monazite (Mnz), Phlogophite (Phl), Cerite (Crt), Illite (Ill), Hematite (Hem), Biotite (Bt), with abbreviation according to IMA-CNMNC [37].

The other sample containing different Th and REE-bearing minerals such as thorutite

(Th, U,Ca)$Ti_2(O,OH)_6$ in sample MV2, and thorite $Th(SiO_4)$ in sample MV4 [41]. The occurrences of thorutite are associated with autunite $Ca(UO_2)_2(PO_4)_2 \cdot 10\text{-}12H_2O$. Thisis a special case for thorium and uranium mineralization. The other minerals containing REE, especially Ce, is Chevkinite-(Ce): $Ce_4(Ti,Fe^{2+},Fe^{3+})_5O_8(Si_2O_7)_2$. This mineral is very rarely found in other mineralization.

Analysis using AMICS software resulting in identification of some minerals containing Th and REE such as britholite, monazite, thorutite, thorite, cerite, aeschynite, and chevkinite-Ce. These minerals are associated with apatite, actinolite, illite, hematite, pyrite, titanite, and some other light minerals. The distribution of these minerals is found in form of oriented minerals and scattered in ore bodies. The complete result of AMICS and the percentage of the mineral in the ore are shown in Table 5.

Table 5. Mineral composition resulted by AMICS.

Minerals	MV0 (wa.%)	MV2 (wa.%)	MV3 (wa.%)	MV4 (wa.%)	MV6 wa.%)	MV7 (wa.%)
Britholite*	84.96	-	2.5	-	66.99	9.9
Monazite*	-	-	14.43	-	1.36	-
Thorutite*	-	5.1	-	-	-	-
Thorite*	-	0.21	-	8.1	-	-
Cerite*	-	-	0.17	-	0.09	-
Aeschynite*	-	-	0.05	-	-	-
Chevkinite-Ce		0.21				
Apatite	-	27.28	-	-	0.02	-
Actinolite	-	-	-	-	1.59	19.34
Illite	7.02	-	50.31	46.92	-	-
Hematite	0.74	0.43	2.27	37.14	8.40	43.92
Pyrite	0.45	19.24	-	-	0.37	-
Pyroxene	0.03	9.46	0.02	-	0.02	0.24
Phlogopite	0.34	-	9.91	-	-	-
Biotite	1.05	10.2	-	-	-	-
Titanite	-	19.15	3.95	-	1.14	0.6
Zeolite	-	-	-	-	14.44	15.42
Sericite	-	-	-	-	5.91	6.71
Others	5.41	8.72	16.39	7.84	2.81	3.87

DISCUSSION

Th and REE become the new exploration interest in the last decade in Indonesia. These minerals' prospect area for this mineral is Mamuju Area, which was explored since 2012 [3,5,26]. The distribution of prospect area covers for instance in the Adang Volcanic Complexes [42]. Some sectors were identified as exploration targets of radioactive minerals exploration areas based on radiometric anomaly [43]. One of the prospective sectors with high radioactivity and Th anomaly is the Hulu Mamuju Sector in the center of the Adang Volcanic circular. The Th and REE enrichment were found in the mineralization area with the fracture filling system. Most of the mineralization was identified as a fracture filling zone with various fracture patterns, with fracturation zone thickness ranging from 1.5-4 m. The structure zone has a radial pattern following the volcanic main structure. Eight mineralization zones were identified and some parts of these were characterized by the anomalous value of radiometric from 46.4 to > 1,100 μSvh^{-1}. The representative sample from every mineralization zone was collected and analyzed with several methods.

The geochemistry analysis using XRF and ICP-MS shows the condition of samples is strongly altered. Th content in all of the samples elevated thousand times from 1.1 to 7.4 % of Th. This value is followed by uranium (U), zirconium (Zr), and the light REE elements such as yttrium (Y), lanthanum (La), cerium (Ce), praseodymium (Pr), neodymium (Nd). The value of heavy REE is also elevated hundred times, such as gadolinium (Gd), dysprosium (Dy), and erbium (Er). The high content of Th and U caused the gamma-ray dose is very intensive and the radiometric method is strongly useful for identifying the surface and subsurface mineralization [44].

The mineralization conditions of Th and REE are based on the trace element ratio La/Yb vs total REE and Y (TREY), indicating the mineralization influence by the magmatism fluid processes such as the formation of carbonate magma (La/Yb>20). The TREY content is very abundant (>600 ppm) [45]. A high ratio of La/Yb and TREY shows the mineralization is an enrichment of carbonatite or peralkaline magma (Fig. 12).

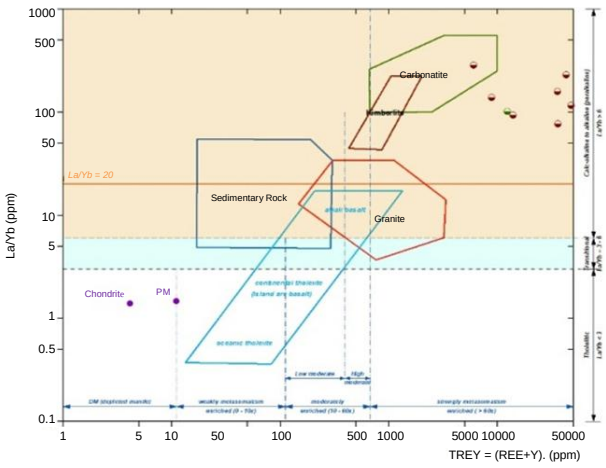

Fig. 12. Trace elements ratio of La/Yb vs TREY showing the ratio is >20 and TREY >600 [45].

The comparison of samples with molar content (FeO + MnO)/ MgO has a value of 2.9-19.0 with a requirement of > 1 and CaO/(CaO + MgO + FeO + MnO) has a value of 0.02-0.2 with a requirement of < 0.5 is a special condition that can

grouped into Fe enrichment in carbonated magmas. CaO, MgO and $FeO+Fe_2O_3+MnO$ diagrams (Fig. 13). The latter shows that all samples are enriched carbonatite fluid which are classified as "ferro-carbonatite" [46]. The "ferro-carbonatite" ore deposits are the first identified of Th and REE mineralization in Indonesia, that only applied for the special condition of ore with the modal mineralogy is only to carbonatites with truly Fe-rich, to those carbonatites with the main Fe-rich and low Mg carbonate mineral.

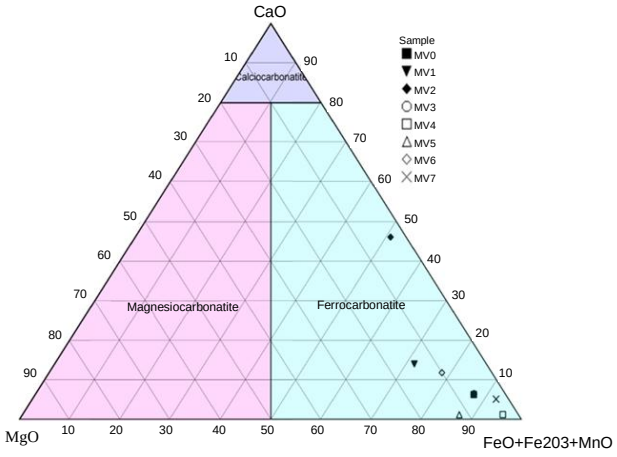

Fig. 13. Ternary diagram correlation of CaO, MgO, and $FeO+Fe_2O_3+MnO$ on the classification of enriched carbonatite magma [46].

Micrograph analysis shows all the samples are altered and dominated by opaque minerals (hematite) on the edge, and mineral aggregates of apatite group minerals (britholite), zeolite, sericite, aegirine, and small mineral on the inner side of the vein. The samples with high content of thorium and REE was scanned to get the distribution of the element composition in the minerals. Elemental mapping of minerals can be describing the precise distribution of each element. The elemental mapping using the micro-XRF method shows the distribution of each minerals elements and composite, especially the distribution of thorium and REE [10,29,30,47]. The spectrum in every pixel with 20 µm size can be identified in detail for distribution of elements composites.

The result of micro-XRF processes by AMICS analysis resulting in Th-TREY-rich and Fe-rich minerals with strictly different distribution. Th and TREY mostly accumulated as aggregates of apatite which is identified as britholite [40,48], monazite, thorutite, thorite, and cerite associated with apatite, actinolite, Illite, hematite, pyrite, and some light minerals.

The genesis of britholite-Ce minerals is usually found in alkaline, acid, and carbonatitic rocks, formed in the late magmatic process [40,49]. Monazite is also found in some samples. Monazite has a high content of Th found dominantly in MV3 associated with carbonate REE such as aeschynite. This mineral occurrence indicated the low temperature of mineralization [50].

Thorutite is a very rare mineral found in Indonesia, this mineral has a high content of Th and U, but is often found in minerals where that Th and U are associated with REE [41]. In this report, the sample of MV2, this mineral associated with secondary U-mineral, which is autunite. The physical properties of thorutite and autunite are very difficult to separate by the naked eye or photomicrograph, but they can be identified in AMICS software. The other minerals containing Th are thorite associated with thorutite with 8.1 wa.% area or 9.66 wt.% in the sample. This is the indication of low temperature and multiple processes of mineralization. The distribution of Th and REE-bearing minerals are covered by the oxide mineral.

The occurrences of thorite, thorutite, britholite, cerite, and aeschynite are indications of several stages of mineralization. The enrichment of Th and REE-minerals supposed mineralization begins with the occurrences of carbonatite magma with high content of high field strength elements (HFSE) [51] and followed by a hydrothermal alteration process which produces minerals that form at low temperatures [52].

CONCLUSION

The Adang Volcanic Complexes are composed of undersaturated silica alkaline rocks that have a high radiometric dose rate, especially in Hulu Mamuju Sector. The high radiometric dose rate shows the mineralization containing radioactive elements associated with other valuable elements (Zr, Ti, P, and REE) that have strictly fault-hosted or vein-type mineralization, whereas the NW-SE and NE-SW strike-slip normal faults play an important role for favorable mineralization zone.

Th and TREY concentrations are extremely high in the samples, which are 11,550-74,480 ppm and 6,244.15-48,036.87 ppm, respectively. Geochemical analysis of major and trace elements showing the mineralization is significantly influenced by the carbonatite process and classified to ferro-carbonatite mineralization.

The analysis using µXRF for elemental mapping with small pixel and completed by AMICS can figure out the detailed Th and TREY-bearing minerals, which are identified as britholite $((Ce,Ca)_5(SiO_4)_3OH)$, aeschynite $(Ce,Ca,Fe,Th)(Ti,Nb)_2(O,OH)_6$, cerite $(Ce,Ca)_9(Mg,Fe)(SiO_4)_3(HSiO_4)_4$

$(OH)_3$, monazite (REE,Th(PO_4)), chevkinite-Ce ($Ce_4(Ti,Fe^{2+},Fe^{3+})_5(Si_2O_7)O_8$), thorite (Th($SiO_4$)), and thorutite $(Th,U,Ca)Ti_2(O,OH)_6$ associated with other minerals such as pyrite, actinolite, apatite, ilmenite, hematite, zircon, titanite and ankerite. The mineral occurrences and their association indicated the mineralization probably form as the late phase of magmatism, with occurrences of carbonatite magma containing high field strength elements (HFSE) continued by hydrothermal mineralization and alteration process.

ACKNOWLEDGMENT

Special thanks to Mr. Yarianto and Heri Syaeful for the opportunity and National Nuclear Energy Agency for the research funding.

AUTHOR CONTRIBUTION

Conceptualization, I. G. Sukadana, F. Pratiwi, A. Harijoko and I. W. Warmada; methodology, I. G. Sukadana, F. Pratiwi, A. W. Yogatama and T. B. Adimedha; validation, I. W. Warmada and A. Harijoko; formal analysis, I. G. Sukadana, T. B. Adimedha and A. W. Yogatama; investigation, I. G. Sukadana and T. B. Adimedha; resources I. G. Sukadana, F. Pratiwi, A. W. Yogatama and T. B. Adimedha; data curation, I. G. Sukadana, F. Pratiwi, A. W. Yogatama and T. B. Adimedha; writing-original draft preparation, I. G. Sukadana, T. B. Adimedha, F. Pratiwi; writing-review and editing, I. G. Sukadana, F. Pratiwi, A. W. Yogatama, T. B. Adimedha. All authors read and approved the final version of this manuscript.

Availability of data and materials

Topography and elevation data were generated from Digital Elevation Model Nasional (https://tanahair.indonesia.go.id/demnas/#/demnas)

REFERENCES

1. T. Unak, Prog. Nucl. Energy **37** (2000) 137.
2. H. Syaeful, K. S. Widana, I. G. Sukadana *et al.*, *Rare Earth Element Exploration in Indonesia*, Proceedings of Sundaland Resources 2014 MGEI Annual Convention (2014) 205.
3. H. Syaeful, I. G. Sukadana and A. Sumaryanto, Atom Indones. **40** (2014) 33.
4. I. G. Sukadana, I. W. Warmada, A. Harijoko *et al.*, *The Application of Geostatistical Analysis on Radiometric Mapping Data to Recognized the Uranium and Thorium Anomaly in West Sulawesi, Indonesia,* IOP Conference Series: Earth and Environmental Science **819** (2021) 012030.
5. I. G. Sukadana, H. Syaeful, F. D. Indrastomo *et al.*, J. East China Univ. Technol. **39** (2016) 39.
6. P. H. Koch, C. Lund and J. Rosenkranz, Miner. Eng. **136** (2019) 99.
7. R. D. Barker, S. L. L. Barker, S. A. Wilson *et al.*, Econ. Geol. **116** (2021) 803.
8. Q. Li, X. Hu, J. Hao et al., Chemosphere **249** (2020) 126143.
9. D. Savira, M. A. Gunawan, W. A. Draniswari *et al.*, IOP Conf. Ser. Earth Environ. Sci. **830** (2021) 1.
10. S. Flude, M. Haschke and M. Storey, Mineral. Mag. **81** (2017) 923.
11. A. Guntoro, J. Asian Earth Sci. **17** (1999) 79.
12. B. Situmorang, *The Formation of the Makassar Basin as Determined from Subsidence Curves*, 11th Annual Convention Proceedings **I** (1982) 83.
13. S. C. Bergman, D. Q. Coffield, J. P. Talbot *et al.*, Geol. Soc. Spec. Publ. **106** (1996) 391.
14. M. Polv, R. C. Maury, H. Bellon *et al.*, Tectonophysics **272** (1997) 69.
15. Y. S. Yuwono, R. C. Maury, R. Soeria-Atmadja, *et al., Tertiary and Quaternary Geodynamic Evolution of South Sulawesi: Constraints from the Study of Volcanic Units,* Proceedings PIT XVI Ikatan Ahli Geologi Indonesia (1987) 32.
16. M. A. Elburg and J. Foden, Geochim. Cosmochim. Acta **63** (1999) 1155.
17. R. Hall, I. R. Cloke, S. Nur'aini *et al.*, Pet. Geosci. **15** (2009) 147. (in Indonesian)
18. A. Maulana, K. Watanabe, A. Imai *et al.*, Procedia Earth Planet. Sci. **6** (2013) 50.
19. G. Shaban, Fadlin, B. Priadi *et al.*, Indones. J. Geosci. **8** (2021) 39.
20. W. A. Draniswari, S. I. T. Kusuma, T. B. Adimedha *et al.*, Eksplorium **41** (2020) 73. (in Indonesian)
21. H. Schmeling and N. Arndt, Earth Planet. Sci. Lett. **472** (2017) 95.
22. K. A. Smart, S. Tappe, A. Ishikawa *et al.*, Geochim. Cosmochim. Acta **248** (2019) 311.
23. N. Ratman and S. Atmawainata, Peta Geologi Lembar Mamuju, Sulawesi, Bandung (1993).

24. I. G. Sukadana, A. Harijoko and L. D. Setidjadji, Eksplorium **36** (2015) 31. (in Indonesian)
25. F. D. Indrastomo, I. G. Sukadana, A. Saepuloh, *et al.*, Eksplorium **36** (2016) 71. (in Indonesian)
26. I. G. Sukadana and H. Syaeful, *Uranium Exploration in Sulawesi*, Proceedings Seminar on MGEI 8th Annual Convention, Bandung (2016) 117.
27. W. Keyser, C. L. Ciobanu, N. J. Cook *et al.*, Precambrian Res. **324** (2019) 170.
28. A. Cousin, V. Sautter, V. Payré *et al.*, Icarus **288** (2017) 265.
29. P. M. Wróbel, S. Bała, M. Czyzycki *et al.*, Talanta **162** (2017) 654.
30. W. Tefera, T. Liu, L. Lu *et al.*, Ecotoxicol. Environ. Saf. **193** (2020) 110245.
31. H. Samalehu, A. Idrus, N. I. Setiawan *et al.*, Bull. Iraq Nat. Hist. Mus. **16** (2021) 301.
32. J. Dostal, Resources **6** (2017) 34.
33. R. L. Rudnick and S. Gao, Composition of the Continental Crust, 2nd ed., Elsevier Ltd. (2003).
34. S. S. Sun and W. F. McDonough, Geol. Soc. Spec. Publ. **42** (1989) 313.
35. C. Wei, C. Xu, M. Deng *et al.*, Ore Geol. Rev. **141** (2022) 104654.
36. P. Uher, M. Ondrejka, P. Bačík *et al.*, Lithos **236-237** (2015) 212.
37. L. N. Warr, Mineral. Mag. **85 (**2021) 291.
38. D. Hoehnel, W.U. Reimold, U. Altenberger *et al.* J. African Earth Sci. **138** (2018) 264.
39. W. A. Draniswari, F. Pratiwi, N. Ngadenin *et al.*, Eksplorium **42** (2021) 77. (in Indonesian)
40. D. C. Noe, J. M. Hughes, A. N. Mariano *et al.*, Zeitschrift für Krist. **206** (1993) 233.
41. J. C. M. de Hoog, M. J. van Bergen, Mineral. Mag. **61** (1997) 721.
42. I. G. Sukadana and H. Syaeful, *Implication of Hydrothermal Process on Radioactive and Rare Earth Element Enrichment in Mamuju, West Sulawesi*, Proceedings Joint Convetion Malang, HAGI - IAGI - IAFMI - IATMI (JCM 2017), Malang (2017).
43. I. Rosianna, E. D. Nugraha, H. Syaeful *et al.*, Geoscience **10** (2020) 1.
44. K. Horie, Y. Tsutsumi, M. Cho *et al.*, Phys. Chem. Earth **35** (2010) 284.
45. C. J. Allegre and G. Michard, *The Geochemical Fractionation of Trace Elements*, D. Reidel Publishing Company, Dordrecht, Holland (1974).
46. J. Gittins and R. E. Harmer, J. African Earth Sci. **25** (1997) 159.
47. D. Genna, D. Gaboury, L. Moore *et al.*, J. Geochem. Explor. **108** (2011) 131.
48. O. Terra, F. Audubert, N. Dacheux *et al.*, J. Nucl. Mater. **354** (2006) 49.
49. R. Oberti, L. Ottolini, G. Della Ventura *et al.*, Am. Mineral. **86** (2001) 1066.
50. L. Torró, C. Villanova, M. Castill *et al.*, Mineral. Mag. **76** (2012) 393.
51. S. Y. Jiang, R. C. Wang, X. S. Xu *et al.*, Phys. Chem. Earth **30** (2005) 1020.
52. T. H. DeFerreira, L. A. R. de Oliveira, L. E. D. Amorim *et al.*, Geochem. **81** (2021) 125810.